Catal Lett (2016) 146:1808–1818
DOI 10.1007/s10562-016-1810-x

Lanthanum and Cesium-Loaded SBA-15 Catalysts for MMA Synthesis by Aldol Condensation of Methyl Propionate and Formaldehyde

Yanan Wang[1] · Ruiyi Yan[2] · Zhaopo Lv[2] · Hui Wang[2] · Lei Wang[2] · Zengxi Li[1] · Suojiang Zhang[2]

Received: 17 February 2016 / Accepted: 8 July 2016 / Published online: 19 July 2016

Abstract Aldol condensation of methyl propionate (MP) and formaldehyde (FA) is a green and sustainable route to synthesize methyl methacrylate (MMA). In this work, lanthanum and cesium-loaded SBA-15 acid–base bifunctional catalysts for aldol condensation have been prepared by wetness impregnation method to maximize the yield of MMA. With the investigation of the relationship between the properties of catalysts and the catalytic performance, the appropriate acid–base sites for this reaction were provided. The results showed that La existed as $LaONO_3$ on the catalysts and could constitute additional Lewis acid sites on the catalysts. The Cs-0.1La/SBA-15 (with La content of 0.1 %) exhibited higher catalytic activity than the other La-containing catalysts because of the higher density of medium base sites and medium acid sites. The catalysts calcined at 450 °C performed well on this reaction due to the formation of medium base sites on the catalysts as well as the big surface area around 400 m^2/g and uniform pore size at 6 nm. When the MP/FA molar ratio was 1/1, the conversion of MP was 29.2 % and the selectivity of MMA could reach 90.4 %.

Graphical Abstract

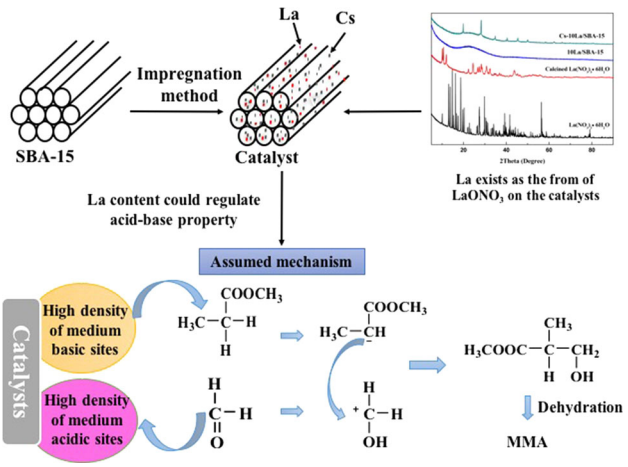

Keywords Lanthanum-loaded · Aldol condensation · Acid and base properties

1 Introduction

Methyl methacrylate (MMA) is a high-value polymer intermediate, which is widely used for organic glass (polymethyl methacrylate), acrylic fibers, plastics, paint, and lustering agent. The traditional way of producing MMA is the Acetone Cyanohydrin process (ACH), which is unsustainable and environmentally unfriendly. Therefore, numerous trials had been made to prepare MMA with

Electronic supplementary material The online version of this article (doi:10.1007/s10562-016-1810-x) contains supplementary material, which is available to authorized users.

✉ Hui Wang
huiwang@ipe.ac.cn

✉ Suojiang Zhang
sjzhang@home.ipe.ac.cn

[1] School of Chemistry and Chemical Engineering, University of Chinese Academy of Sciences, Beijing 100049, People's Republic of China

[2] Beijing Key Laboratory of Ionic Liquids Clean Process, Key Laboratory of Green Process and Engineering, State Key Laboratory of Multiphase Complex Systems, Institute of Process Engineering, Chinese Academy of Sciences, Beijing 100190, People's Republic of China

hydrocarbon routes [1, 2]. Researchers divided these routes into C_2, C_3 and C_4 routes according to their feedstocks. C_2 route refers to the one using ethylene as the raw material [3]. α-MMA route is the modified C_2 route which involves two steps by converting ethylene, CO, and methanol to MMA. Carbonylation of propylene is a better way than the ACH process, both of which are based on C_3 feedstocks, but the life of catalysts for the oxidation of *iso*butyric acid is short. In the C_4 route, *iso*propylene is transformed to MMA, but the processing is too complicated through two steps of oxidation [4–8]. Compared with the other routes, the α-MMA route has distinctive advantages in rich materials, short routes, and environmentally friendly. Vapor-phase aldol condensation between methyl propionate and formaldehyde is the key step in the α-MMA route, but the catalysts available for this reaction exhibit low yields. Researchers firstly studied the activity of V-Si-P catalysts for the aldol condensation [9]. Silica-supported alkali and alkaline earth metal hydroxides catalysts were prepared and the catalytic performances in the production of MMA were investigated by Ai [10]. They found that the $CsOH/SiO_2$ had good catalytic activity, with the yield of MMA reaching 13 % when MP/FA = 0.2, but the catalytic activity decreased slowly with the time-on-stream. Li et al. [11] chose the modified Zr–Mg–Cs/SiO_2 catalysts to get a higher yield of MMA, but the selectivity was still low (∼80 %). Using SBA-15 supported cesium catalyst, selectivity of MMA could reach 93 %, but with low conversion, around 26 % [12]. The mechanism of aldol condensation reported by Gogate [13] showed that both acid and base sites in the catalysts were active for this reaction. Thus, the key issue of this reaction was the development of suitable acid–base bifunctional catalysts and balance the acid and base sites to maximize the yield of MMA [3].

Recently, rare earth compounds, especially lanthanum compounds, have been widely used in catalysts [14, 15]. It is widely reported that lanthanum-containing compounds were excellent catalysts for many condensations [16–21]. The lanthanum-containing catalysts showed excellent activity in these reactions due to the property of alkalinity and thermal stability of lanthanum oxide [16, 22, 23]. Kumar et al. [24] had previously synthesized ceria–lanthanum based catalysts for the preparation of dimethyl carbonate. The yield was significantly high when the molar ratio of Ce/La was 1/4, which indicated that the density of basic sites and the total amount of acidic sites could be enhanced by increasing the amount of lanthanum. In the research of Nguyen [25], lanthanum orthophosphate catalysts were active and selective for the dehydration of light alcohols. The lanthanum phosphates have both Brønsted and Lewis acidic sites. The Lewis acid sites related to the lanthanum cations played an important role in this reaction. In a word, the lanthanum-containing catalysts could change the acid–base properties of catalysts and change the catalytic performance further. However, the relationship between the catalytic mechanism and the acid–base sites formed by La had not been reported. Furthermore, lanthanum-supported catalysts have not been used for MMA synthesis by aldol condensation of MP and FA so far.

Ordered mesoporous siliceous materials such as SBA-15 have recently received growing attention due to their appealing textural properties, high surface area, appreciable thermal and hydrothermal stability, so the SBA-15 was selected as the support.

In this work, the Cs-La-supported SBA-15 catalysts were prepared by the impregnating method. The Cs-xLa/SBA-15 catalysts were characterized by NH_3 and CO_2-Temperature Programmed Technique, X-ray Diffraction, Ultra-high Resolution Field Emission Scanning Electron Microscope, Fourier Transform Infrared Spectrometer and N_2 Physisorption. The effects of La content and calcination temperature of the catalysts on the catalytic activity for the aldol condensation of MP and FA were studied in a fixed-bed reactor. Based on the discussion of the relationship between the properties of catalysts and the catalytic performance, the appropriate acid–base sites for this reaction were provided.

2 Experiment Section

2.1 Catalyst Preparation

Cesium nitrate (99.9 %) was industrial grade and purchased from Hubei Baijierui Advanced Materials CO. LTD. Poly (ethylene oxide)-block-poly (propylene oxide)-block-poly (ethylene oxide) triblock copolymer (P123) was purchased from Aldrich. Lanthanum nitrate hexahydrate (corresponding La_2O_3 content ≥44.0 %) and tetraethoxysilane (TEOS) are analytical reagents. Methyl propionate (≥99.0 %), paraformaldehyde (≥94.0 %) and methanol (≥99.0 %) are analytical reagents.

The SBA-15 material was prepared according to the method reported by Zhao et al. [26]. TEOS was used as the silica source and P123 as the template. 2.0 g of P123 was dissolved in 60 g of HCl (2 mol/L) and 15 g of H_2O, and the mixture was stirred for 3 h to get a clear solution (solution A) at 40 °C. Then 4.35 g of TEOS was dropped to solution A and then stirred vigorously for 24 h at 40 °C. Afterwards it was transferred into an autoclave and aged for 24 h. The resultant substance was filtered, washed, dried and calcined at 550 °C for 6 h to get SBA-15.

Cs-La/SBA-15 catalysts with different La-loadings and the same Cs-loading (the Cs element content was 15 % which was based on weight percent of the supports [12]) were prepared by wetness impregnation method. 1.101 g

$CsNO_3$ and 1.29 g $La(NO_3)_3{\cdot}6H_2O$ (10 wt%) were dissolved in 30–35 mL water to get a clear solution (solution B) at room temperature. The solution B was dripped to 5 g SBA-15 solid in an Erlenmeyer flask, then the mixture was oscillated for 12 h at 40 °C. The resulting material was dried at 100 °C in air for 12 h and calcined in air at 450 °C for 5 h. These samples were marked with Cs-xLa/SBA-15, where x was the amount of La in the catalysts (x = 0, 0.01, 0.05, 0.1, 0.5, 1, 5, 10 wt%).

2.2 Catalyst Characterization

X-ray diffraction (XRD) patterns were obtained in an X' Pert PRO MPD diffractometer operating at 45 kV and 200 mA with CuKα radiation. The intensity of diffraction was measured by increasing angle (2θ) from 5^o to 90^o at a rate of 15 ^{o}/min.

The amount of cesium and lanthanum in the Cs-La/SBA-15 catalysts were quantified by inductively coupled plasma (ICPE9000) from SHIMADZU.

HITACHI Ultra-High Resolution Field Emission Scanning Electron Microscope (UHR FE-SEM) was used to get the images of catalyst samples with the operation voltage of 5.0 kV.

The BET specific surface area, the pore volume, and pore size were obtained from nitrogen absorption isotherm at liquid nitrogen temperature in a Micrometrics ASAP 2460 apparatus. Before measurement, the samples were degassed at 150 °C for 4 h.

Fourier Transform Infrared Spectrometer (FT-IR Nicolet 380) was used to get infrared spectra of the catalyst samples by using potassium bromide-disk technique. Every time about 2 mg sample was added to 200 mg KBr to prepare the disks for testing. The surface acidity of the catalysts was investigated by means of studying pyridine adsorption on a Nicolet 6700 FTIR spectroscopy in situ equipped with a cell. The samples that had been pressed into a plate were put into the cell, and pretreated at 150 °C under vacuum for 30 min to remove the impurity. After cooling to 30 °C, the cell was scanned and the obtained data was used as the background. Then pyridine vapor was introduced into the cell for 30 min to reach equilibrium. Then the cell was scanned after being vacuumed for 10 min and recorded at 50, 100, 200 and 300 °C. The background has been subtracted from the spectrum of the corresponding catalyst adsorbed with pyridine.

The acid and base properties were obtained on an Auto Chem II 2920 Chemisorption Analyzer from Micrometrics by the method of temperature programmed desorption. For acidity measurements, about 30 mg samples were placed in a quartz tube and pretreated in a helium flow at 120 °C for 30 min. Then the temperature was reduced to 50 °C. A mixture of 10 % NH_3-He was passed through the samples for 90 min at 50 °C. Then the samples were purged with pure helium at 50 °C for 30 min. When the baseline was stable, the NH_3 desorption rate was monitored and gave one measurement every 1.0 s by the thermal conductivity detector in helium flow at a heating rate of 10 °C/min to 500 °C. The basicity of the catalysts was measured using 10 % CO_2-He mixtures and the processing was the same as that of the NH_3-TPD.

2.3 Catalytic Activity Measurement

The reaction was measured in a fix-bed reactor at atmospheric pressure in nitrogen environment. The reactor was made of a stainless steel tube placed vertically in an electric furnace, which was 42 cm long, 0.8 cm outside diameter and 0.5 cm inside diameter. 0.8 mL of catalyst was put exactly in the middle of the tube with the quartz sands filled both ends. The mixed solution of MP, FA and methanol (the molar ratio of MP/FA/methanol was 1/1/1.5) was fed in from the top of the reactor by an advection pump. The methanol was used as a solvent to depolymerize the paraformaldehyde feed. The liquid samples were collected after 180 min on stream and then collected every 120 min. Gas samples were analyzed on-line and liquid products were analyzed off-line by gas chromatography (GC) using an Agilent 7890A GC apparatus with *n*-heptane as an internal standard and sample detection was accomplished with a Flame Ionization Detector (FID). The activity of the catalysts was measured by testing the conversion of MP and the selectivity and yield of MMA, which were calculated using Eqs. 1, 2, 3.

$$\text{Conversion of MP} = \frac{\text{MP}_{\text{in,mol}} - \text{MP}_{\text{out,mol}}}{\text{MP}_{\text{in,mol}}} \times 100\% \quad (1)$$

$$\text{Selectivity of MMA} = \frac{\text{MMA}_{\text{out,mol}}}{\text{MP}_{\text{in,mol}} - \text{MP}_{\text{out,mol}}} \times 100\% \quad (2)$$

$$\text{Yield of MMA} = \text{Conversion of MP} \times \text{Selectivity of MMA} \quad (3)$$

3 Results and Discussion

3.1 Catalyst Characterization

3.1.1 Element Analysis

The Element content of the catalysts was investigated by ICP and the result was shown in the Table 1. The calculated contents of Cs and La were slightly greater than the actual contents, which proved that although some loss of elements have happened during the catalyst preparation,

Table 1 The Element content of the Cs-xLa/SBA-15 catalysts calcined at 450 °C

Catalyst	Calculate value (wt%)		Measured value (wt%)	
	Cs	La	Cs	La
Cs/SBA-15	15	0	11.2	0
Cs-0.01La/SBA-15	15	0.01	10.0	0.0072
Cs-0.1a/SBA-15	15	0.1	11.6	0.080
Cs-1La/SBA-15	15	1	11.0	0.69
Cs-10La/SBA-15	15	10	9.9	4.0

the Cs and La were both impregnated on the catalysts. The contents of Cs were about 10–11 %, and the contents of La increased with the calculated contents. EDS images of La on the Cs-xLa/SBA-15 catalysts were shown in Fig. S1. La were homogeneous distributed on the surface of SBA-15 when the content of La was less than 5 %. However, La distributed heterogeneously when the La content was 10 %, and La aggregation was observed.

3.1.2 XRD Analysis

The XRD patterns of the Cs-xLa/SBA-15 catalysts with different contents of La were shown in Fig. 1. There were no obvious diffraction peaks related to La compound [27]. Typical diffraction peaks of $CsNO_3$ were observed, as shown by the peaks marked by # in Fig. 1, indicating that Cs existed on the catalysts in the form of $CsNO_3$.

The XRD patterns of the catalysts with different calcination temperatures were shown in Fig. 2. With the calcination temperature increasing, the intensity of the typical diffraction peaks of $CsNO_3$ decreased. The catalysts calcined under 500 °C maintained the complete crystal form

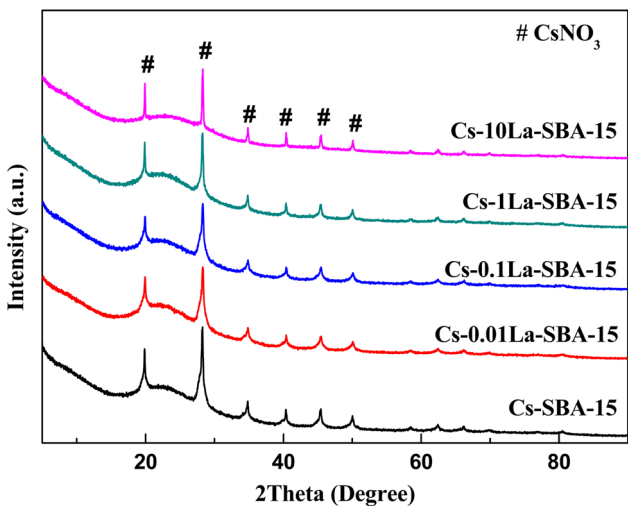

Fig. 1 XRD pattern of the Cs-xLa/SBA-15 catalysts calcined at 450 °C with different La contents

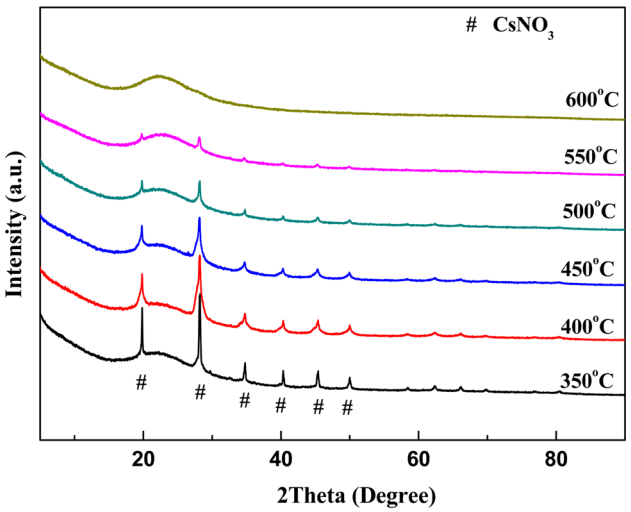

Fig. 2 XRD pattern of Cs-0.1La/SBA-15 catalysts (La content: 0.1 %) with different calcination temperatures

of $CsNO_3$ indicating that Cs existed on the catalysts in the form of $CsNO_3$. It is in accordance with the literature reporting that $CsNO_3$ was decomposed and volatilized above 500 °C [11].

However, diffraction peaks related to La compounds were not present in the patterns. So we calcined the raw material $La(NO_3)_3{\cdot}6H_2O$ and 10La/SBA-15 (content of La was 10 %) at 450 °C. The XRD patterns of $La(NO_3)_3{\cdot}6H_2O$, calcined $La(NO_3)_3{\cdot}6H_2O$, 10La/SBA-15 and Cs-10La/SBA-15 were shown in Fig. 3. The calcined $La(NO_3)_3{\cdot}6H_2O$ at 450 °C showed typical diffraction peaks of $LaONO_3$ (marked by @), indicating that the $La(NO_3)_3{\cdot}6H_2O$ undergone a transformation into $LaONO_3$ when calcined at 450 °C. It is in accordance with the

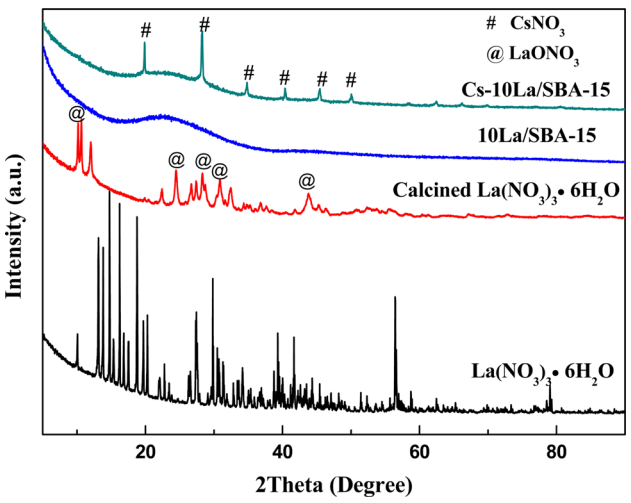

Fig. 3 XRD patterns of $La(NO_3)_3{\cdot}6H_2O$, $La(NO_3)_3{\cdot}6H_2O$ calcined at 450 °C, 10La/SBA-15 calcined at 450 °C and Cs-10La/SBA-15 calcined at 450 °C

literature reporting that the thermal decomposition of $La(NO_3)_3{\cdot}6H_2O$ follows the following steps: the weight loss was about 20 % between 50 and 200 °C which was attributed to the loss of adsorbed and crystal water; $La(NO_3)_3$ was decomposed into La_2O_3 by two steps with 40 % weight loss from 400 to 650 °C. And $LaONO_3$ was proposed as an intermediate phase between La $(NO_3)_3$ and La_2O_3 [28, 29].

The comparison of XRD patterns between 10La/SBA-15 and Cs-10La/SBA-15 showed that the diffraction peaks related to $LaONO_3$ were not present. Taking the element analysis result into consideration, when the calculated value of La on the catalysts was 10 %, the measured value was only 4.0 %. Thus $LaONO_3$ was well dispersed in the channels of SBA-15.

3.1.3 IR Analysis

The IR spectra in the fingerprint of SBA-15 and different La-containing Cs-xLa/SBA-15 samples were shown in Fig. 4. The vibration band at 1079 cm^{-1} was assigned to ν_{as}(Si–O–Si) and the vibration band at 802 cm^{-1} was assigned to ν_s(Si–O–Si) [30, 31]. The two peeks occurred in all the spectra of SBA-15 and Cs-xLa/SBA-15 catalysts and had no evident changes, indicating the Cs and La loaded on the SBA-15 had no influence on the skeletal structure of SBA-15. A band at 1385 cm^{-1} was observed in the Cs-xLa/SBA-15 samples, but not observed in SBA-15. This band can be assigned to the NO_3^- antisymmetric stretching vibrations of N–O [32], indicating the existence of nitrate anion.

The IR spectra in the fingerprint of the Cs-0.1La/SBA-15 samples with different calcination temperatures were shown in Fig. S2. The band intensity of ν_{as}(N–O) decreased, corresponding to the decomposition of $CsNO_3$ and $La(NO_3)_3{\cdot}6H_2O$, in accordance with the XRD results.

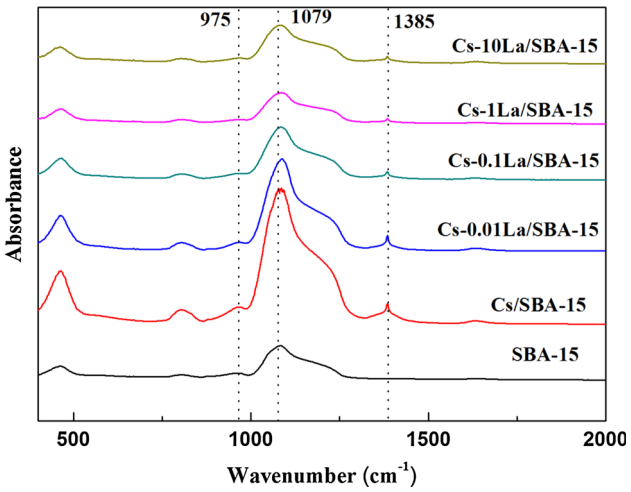

Fig. 4 IR spectra of SBA-15 and Cs-xLa/SBA-15 catalysts calcined at 450 °C with different La contents

3.1.4 BET Specific Surface Area Analysis

The pore size, pore size distribution and specific surface area of SBA-15 and La-containing catalysts were investigated by N_2 adsorption isotherm analyses at liquid nitrogen temperature. The results were shown in Table 2. The BET surface area for the catalysts containing La and Cs are considerably lower than the area for SBA-15. The catalysts containing La and Cs had similar BET surface area and pore volume, thus, an increase in the lanthanum content between 0 and 10 % had no evident influence on the pore surface area and pore volume of the catalysts. The decrease of BET surface area and pore volume was due to the fact that impregnation of Cs on SBA-15 could occupy some channels. In addition, the pore diameters of all the samples were distributed uniformly around 6 nm.

Textural properties and pore size distribution of the Cs-0.1La/SBA-15 catalysts at different calcination temperatures were obtained (Table 3 and Fig. S3). Isotherms belonged to the "type VI" class in the cases of calcination temperatures lower than 500 °C and exhibited a type "H1" hysteresis loop indicating that the catalysts were mesoporous in nature (Fig. S3). The pore size was uniformly distributed around 6 nm. The surface area of these catalysts was in the range of 313–494 m^2/g and decreased in the order of 350, 400, 450, 500 °C. The pore volume of the catalysts also decreased in the same order. The reason for the slightly decrease was that the layer-type $LaONO_3$ was formed [33] and dominated the pore of SBA-15 during the decomposition of $La(NO_3)_3{\cdot}6H_2O$.

When the calcination temperature was above 500 °C, the decomposition and volatilization of $CsNO_3$ happened. The resulting collapse of the SBA-15 structure led to the formation of a bimodal pore size distribution and the swift decline of surface area and pore volume.

3.1.5 Pyridine-FTIR Analysis

Acid species of the Cs/SBA-15 and Cs-0.1La/SBA-15 samples were investigated by the pyridine FTIR spectra after adsorbing pyridine vapor for 30 min. Typical pyridine adsorption peaks referring to Lewis acid sites were shown near 1446 and 1597 cm^{-1} (Fig. 5). The intensity of Lewis adsorption peak at 1446 cm^{-1} in the spectra of Cs-0.1La/SBA-15 was higher than that of Cs/SBA-15. So the presence of La in the catalysts could enhance the amount of Lewis acid sites in the catalysts.

The FTIR spectra of pyridine desorbed at 50, 100, 200, and 300 °C on the Cs-0.1La/SBA-15 and Cs-1La/SBA-15 catalysts were shown in Fig. 6. Generally, pyridine

Table 2 Textural of the catalysts calcined at 450 °C with different La contents

Catalyst	Amount of lanthanum (wt%)	Surface area (m^2/g)	Pore volume (cm^3/g)	Mean pore diameter (nm)
SBA-15	–	964	1.6	6.1
Cs/SBA-15	0	351	0.68	6.0
Cs-0.01La/SBA-15	0.01	349	0.68	6.9
Cs-0.1a/SBA-15	0.1	374	0.72	6.8
Cs-1La/SBA-15	1	370	0.71	6.2
Cs-10La/SBA-15	10	365	0.68	6.7

Table 3 Textural of the Cs-0.1La/SBA-15 catalysts with different calcination temperatures

Calcination temperature of Cs-0.1La/SBA-15 (°C)	Surface area (m^2/g)	Pore volume (cm^3/g)	Pore size (nm)
350	494	0.83	6.5
400	405	0.75	6.9
450	374	0.72	6.6
500	313	0.65	6.9
550	120	0.44	12.6
600	141	0.33	7.7

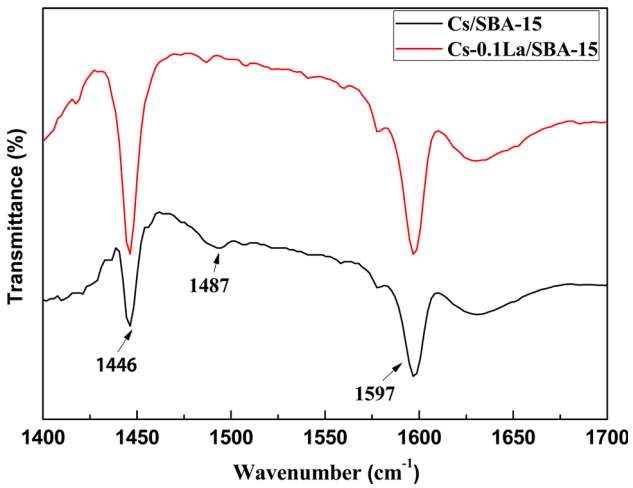

Fig. 5 Pyridine-FTIR spectra for Cs/SBA-15 and Cs-0.1La/SBA-15 catalyst calcined at 450 °C

adsorbed on weak acid sites desorbed at low temperatures and that on strong sites desorbed at high temperatures. The spectra of the two catalysts with pyridine being desorbed at 50 °C showed an obvious peak at 1446 cm^{-1}. Afterwards, this Lewis adsorption peaks disappeared at 100 °C on the Cs-0.1La/SBA-15. However, the Lewis acid sites were strong enough to be detected at 100 °C on Cs-1La/SBA-15. The formation of different strength of Lewis acid sites was considered to be caused by the different La contents. So the lanthanum ions constituted additional Lewis acid sites, the strength of which was slightly higher than the sites constituted by cesium ions.

3.1.6 NH_3–TPD and CO_2-TPD Analysis

TPD studies were performed to identify various acid and base species on the surface of the catalysts. The NH_3-TPD and CO_2-TPD patterns of the Cs-xLa/SBA-15 catalysts with different contents of La were present in Figs. 7, 8. It is evident from the results that varying the La content could induce specific changes in the acid–base characters for each La-supported catalyst. There were three apparent desorption peaks in the CO_2-TPD and NH_3-TPD patterns of Cs-xLa/SBA-15 that were different from each other by their positions, heights and widths, indicating not only the total acidity was different, but also the distribution of the acid strength. The peaks ranged from 100 to 300 °C, from 300 to 480 °C and from 480 to 600 °C, respectively. The higher the desorbed temperature, the stronger the strength of the acid or base sites were [34–36]. The three peaks corresponded to the weak, medium and strong base or acid sites, respectively. The amount of the acid–base sites was summarized in Table 4. Notably, the desorption of water or other components at low temperatures and the decomposition of residual nitrates at temperatures above the calcination temperature have some influence on the TPD result. So the blank experiments were designed to eliminate the influence of water desorption and samples decomposition. And these interferences have been subtracted from the figures and dates shown in the following. The blank experiments processing was the same as the TPD method except that the mixture 10 % NH_3-He (or 10 % CO_2-He) was replaced by He, so that NH_3 or CO_2 was not adsorbed

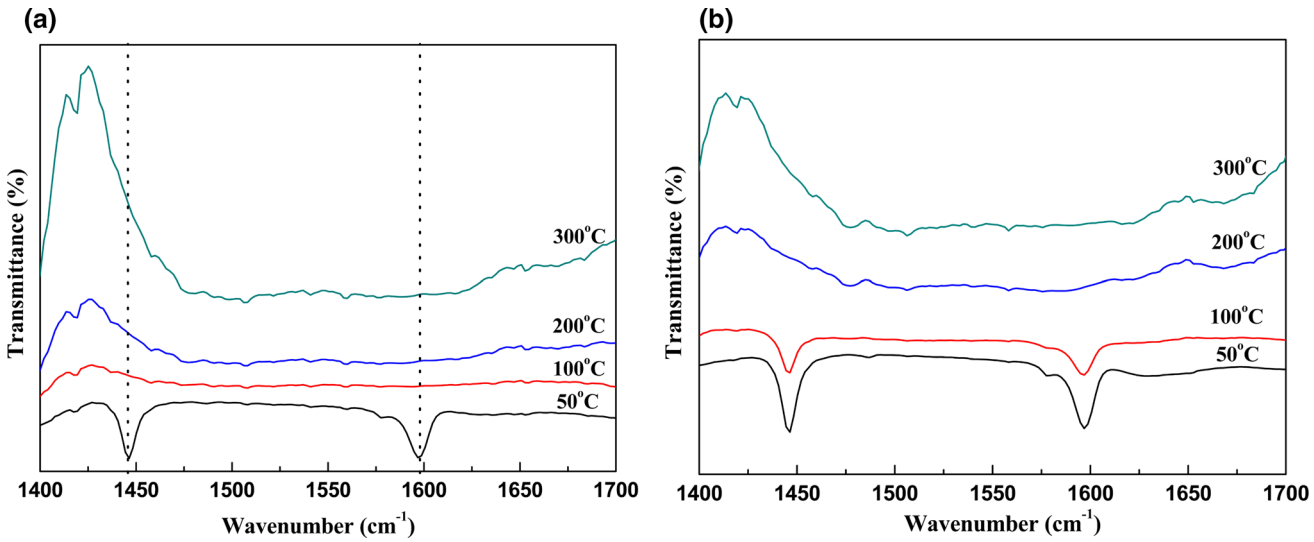

Fig. 6 Pyridine-FTIR spectra as a function of temperature for the Cs-0.1La/SBA-15 (**a**) and Cs-1La/SBA-15 (**b**) calcined at 450 °C

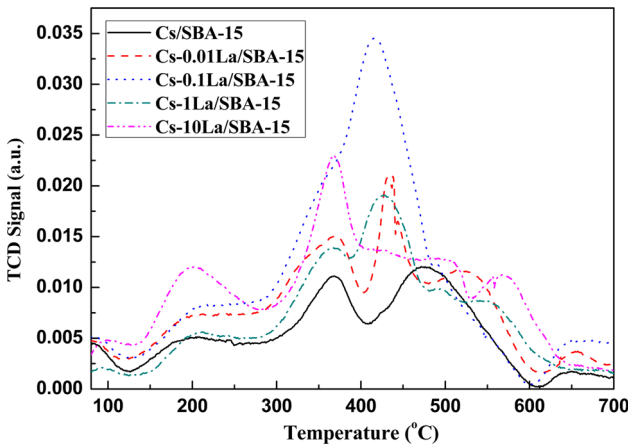

Fig. 7 CO_2-TPD patterns of Cs-xLa/SBA-15 catalysts calcined at 450 °C with different La contents

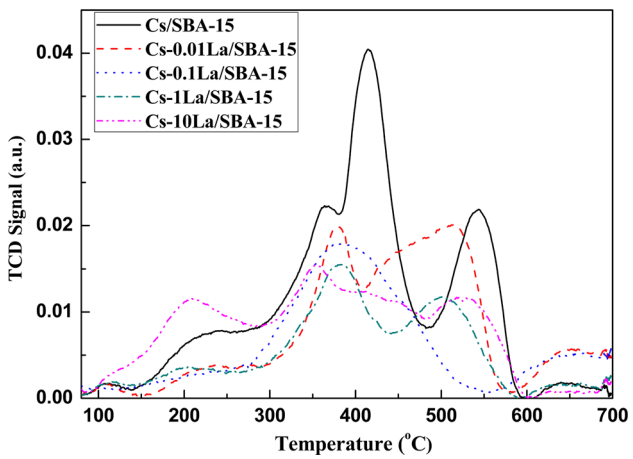

Fig. 8 NH_3-TPD patterns of Cs-xLa/SBA-15 catalysts calcined at 450 °C with different La contents

by samples and the TCD signal results represent for the samples decomposition.

With the increase of the content of La-loading, the density of medium base sites increased firstly and then decreased. The Cs-0.1La/SBA-15 had the highest density of medium base sites among the Cs-xLa/SBA-15 catalysts. The density of weak base sites on the Cs-10La/SBA-15 increased and the peak of medium base sites (around 420 °C) shifted slightly to the low temperature zone (around 370 °C), indicating that the strength of the base sites was weakened because of the increasing of La content.

The NH_3-TPD patterns were similar when the content of La was less than 1 %. However, with the content of La reaching 10 %, the strength of the acid sites reduced and the density of weak acid sites increased. The increasing density of weak acid sites can be attributed to the presence of Lewis acid sites, in agreement with the pyridine-FTIR analysis above. The density of medium acid sites was slightly reduced when La was present in the catalysts. The density of strong acid sites decreased and then increased, and the Cs-0.1La/SBA-15 catalyst had the lowest density of strong acid sites among the Cs-xLa/SBA-15 catalysts.

The CO_2-TPD and NH_3-TPD patterns of catalysts calcined at different temperatures were shown in Figs. 9, 10. The intensity of acid–base sites related to the releasing temperature of CO_2 or NH_3. When the catalysts were calcined below 450 °C, the amount of medium acid sites changed slightly. While the density of medium base sites was increased, which was due to the formation of $LaONO_3$ from the decomposition of $La(NO_3)_3$. When the calcination temperature was higher than 450 °C, medium acid sites and base sites was gradually decreased. It is reported in the

Table 4 Acid–base property of the catalysts calcined at 450 °C with different La contents

Catalyst	Amount of lanthanum (wt%)	Amount of base site (mmol/g)			Amount of acid site (mmol/g)		
		Weak strength (100–300 °C)	Medium strength (300–480 °C)	Strong strength (480–600 °C)	Weak strength (100–300 °C)	Medium strength (300–480 °C)	Strong strength (480–600 °C)
Cs/SBA-15	0	0.136	0.472	0.135	0.111	0.441	0.135
Cs-0.01La/SBA-15	0.01	0.074	0.310	0.124	0.035	0.396	0.200
Cs-0.1a/SBA-15	0.1	0.067	0.684	0.113	0.015	0.469	0.022
Cs-1La/SBA-15	1	0.057	0.343	0.175	0.060	0.267	0.104
Cs-10La/SBA-15	10	0.229	0.402	0.169	0.215	0.314	0.120

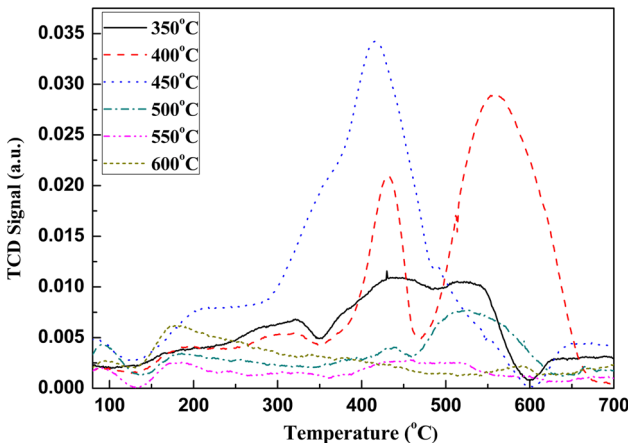

Fig. 9 CO_2-TPD patterns of Cs-0.1La/SBA-15 with different calcination temperatures

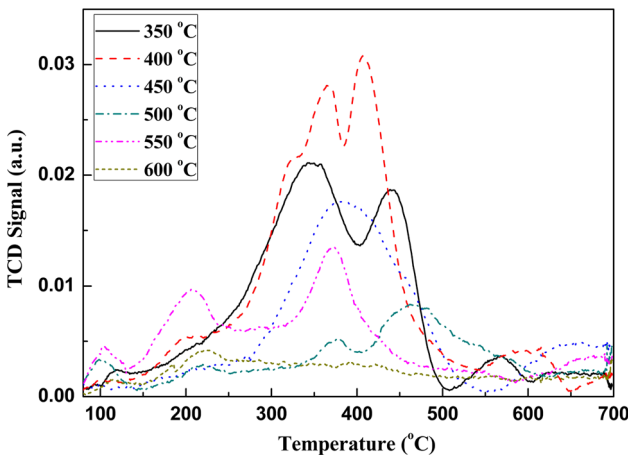

Fig. 10 NH_3-TPD patterns of Cs-0.1La/SBA-15 with different calcination temperatures

literatures [11, 28, 29] that $LaONO_3$ was decomposed to La_2O_3 when calcined higher than 500 °C and $CsNO_3$ was decomposed too, thus the reason for the density reduction of medium acid sites and base sites was the decomposition of $CsNO_3$ and $LaONO_3$.

3.2 Effects of Reaction Temperature on the Aldol Condensation of MP with FA

Temperature had an evident influence on the reaction activity. The performance of Cs/SBA-15 was probed by a fix-bed reactor with the same conditions except the temperature and the results were shown in Fig. 11. The conversion of MP increased by two stage as the temperature increased, while the selectivity of MMA increased firstly and then decreased, reaching plateau value at 330–360 °C. In order to produce MMA in high yield and energy-

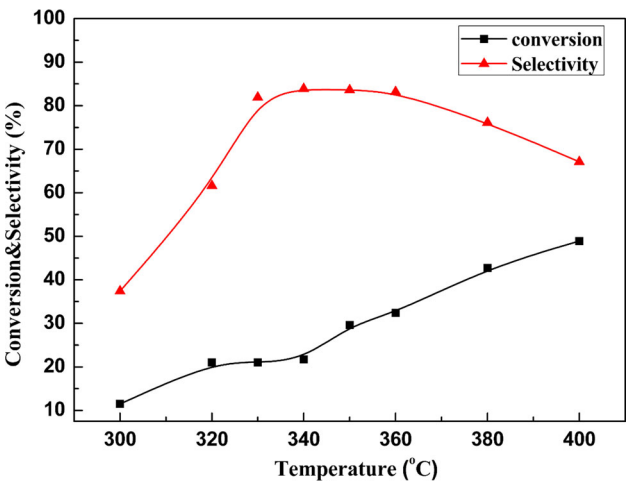

Fig. 11 Catalytic activity of Cs/SBA-15 under different reaction temperatures

efficiently, the catalytic performance was investigated at 350 °C in the following studies.

3.3 Effects of La Content in the Cs-xLa/SBA-15 Catalysts on the Aldol Condensation of MP with FA

The catalytic performance of Cs-xLa/SBA-15 catalysts with different La loadings was investigated. In our previous study, it is reported that the conversion of MP increased rapidly with the loading of Cs and reached a plateau at 15 wt% [11], thus, the Cs content was fixed at 15 wt%. The La content ranged from 0.01 to 10 wt% to investigate the influence of La content on the catalytic activity for the aldol condensation.

The catalytic performances were summarized in Fig. 12. As the La content increased, the selectivity of MMA increased firstly and then decreased, while the conversion remained stable firstly and then decreased. With the La-loading increased from 0 to 0.1 wt%, the selectivity of MMA increased from 86.3 to 90.4 %. If more La was added to catalyst, the selectivity decreased. The conversion of MP would decrease when the content of La was more than 1 wt%. The Cs-0.1La/SBA-15 had the best catalytic activity on this reaction.

Spivey [3] had reported that both acid and base sites were needed for the aldol condensation, and a balance between acid and base sites is also necessary to maximize the reaction yield. MP was activated by basic sites of the catalyst and HCHO by acidic sites, and then a reaction of the two intermediate molecules occurred to form MMA followed by dehydration [13]. Besides, MP could be converted to by products by strong acid sites [10]. In this study, we found that both acid and base sites existed on the catalysts as shown in the TPD results. The relationship between the catalytic behavior and the acid and base sites on the catalysts was investigated, which provided evidence for understanding the catalytic behavior of Cs-xLa/SBA-15 catalysts in the aldol condensation.

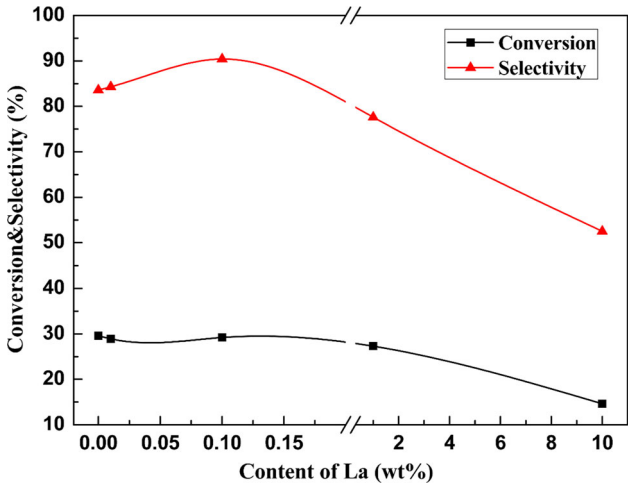

Fig. 12 Catalytic performance of Cs-xLa/SBA-15 catalysts calcined at 450 °C with different La contents

As shown in Figs. 7, 8, the Cs-0.1La/SBA-15 had the highest density of medium base sites and lowest density of strong acid sites than the other catalysts, accounting for maximum selectivity of MMA on Cs-0.1La/SBA-15. It is reported that La loaded on the catalysts could improve both the dispersion of active element and the base property of catalysts [37]. In this reaction, the large amount of base sites and small amount of strong acid sites formed by the La on the catalysts enhanced the activation of MP and weakened the decomposition of MP, thus the selectivity increased. The density of medium acid sites slightly reduced with the introduction of La into catalysts, and there was a little decrease on the conversion of MP. It is concluded that the medium acid sites play an important role on the maintenance of conversion of MP.

When the content of La was higher than 0.1 %, the selectivity decreased owing to the increase of the density of strong acid sites and the decrease of the density of medium base sites on the catalysts, which could weaken the activation of MP and enhance the secondary reaction of MP decomposition. At the same time, the conversion of MP decreased rapidly. There were two reasons for the decrease: Firstly, the increase of the density of strong acid sites led to inappropriate acid–base ratio and carbon deposition would occur, which would decrease the efficiency of the catalysts. Secondly, the La tended to aggregate as shown in the EDS analysis and changed the acid–base property of the catalysts.

In conclusion, when the La content was 0.1 %, the Cs-0.1La/SBA-15 showed superior activity for the aldol condensation. The higher density of medium base sites and smaller density of strong acid sites formed by La on the Cs-0.1La/SBA-15 catalysts enhanced the selectivity of MMA. The adequate density of medium acid sites could improve the conversion of MP.

3.4 Effects of Calcination Temperature of Catalysts on Aldol Condensation of MP with FA

Calcination temperature was an important factor for preparing catalysts since it significantly affected the structure and catalytic properties of catalysts. The Cs-0.1La/SBA-15 were calcined at 350, 400, 450, 500, 550, 600 °C, respectively for 5 h.

Figure 13 showed the evaluation result of the catalyst performance. The conversion of MP increased slightly when calcination temperature was below 400 °C from 25.4 to 29.8 %, and then kept constant around 29 %, however, it

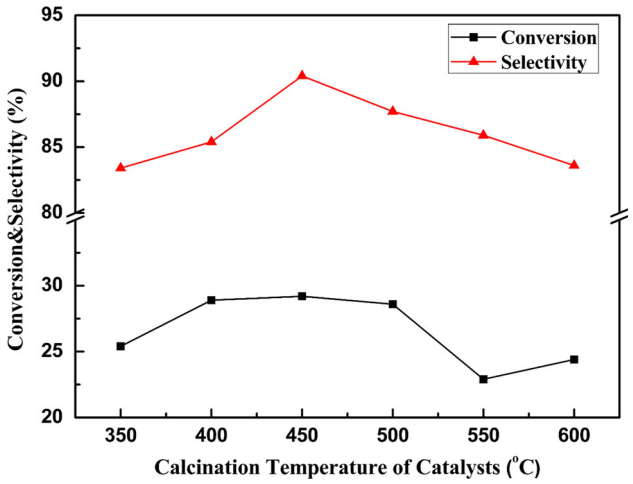

Fig. 13 The effect of calcination temperature of Cs-0.1La/SBA-15 on the performance of the catalysts

decreased rapidly when calcined higher than 500 °C to around 24 %. The selectivity of MMA increased from 83.4 to 90.4 % and then dropped to 83.6 %. The highest selectivity of MMA was obtained at 450 °C.

When the calcination temperature was between 400 and 500 °C, the $La(NO_3)_3$ decomposed into $LaONO_3$. At the same time, the maximum amount of medium base sites was formed, so the introduction of $LaONO_3$ to the catalysts could make contribution to the improvement of density of base sites which could help to promote the main reaction. As a result, the Cs-0.1La/SBA-15 calcined at 450 °C had higher density of the medium base sites and performed better on the aldol condensation with higher selectivity of MMA.

The surface area, pore volume and pore size decreased slightly when calcined below 500 °C, so the change on the pore structure might not be factors for the increase of selectivity but for the maintenance of the conversion. With the partial destruction of the SBA-15 structure and the occupancy of the channels by the decomposed $CsNO_3$, there would be a reduction in surface area, pore volume and the number of acid–base sites. So the decrease of selectivity and conversion with calcination temperature higher than 500 °C could be attributed to the loss of acid–base sites related to the decomposition of the activity component and the formation of mesoporous with different sizes.

4 Conclusions

Cs-xLa/SBA-15 catalysts were prepared by wetness impregnation method. The characterization of the prepared Cs-xLa/SBA-15 catalysts clearly highlights the effect of the La loading dosage and the calcination temperature on the acid–base properties and catalytic performance of these catalysts in the aldol condensation of MP and FA. The pyridine-IR results indicated that the introduction of La to the catalysts could enhance the Lewis acid sites on the catalysts. The higher density of medium base sites and lower density of strong acid sites formed by La on the Cs-0.1La/SBA-15 catalysts enhanced the selectivity of MMA from 86.3 to 90.4 %. In addition, the Cs-0.1La/SBA-15 (La content was 0.1 %) calcined at 450 °C exhibited higher selectivity of MMA due to the existence of $LaONO_3$, which could form high density of the medium base sites on the catalysts. When MP/FA = 1/1, the conversion of MP was 29.2 % and the selectivity of MMA could reach 90.4 %.

Acknowledgments This work was financially supported by National Natural Science Foundation of China (NO. 21406244, 21276267), the Key Program of National Science Foundation of China (NO. 91434203) and the Key Laboratory of Applied Surface and Colloid Chemistry of Shaanxi Normal University.

References

1. Nagai K (2001) Appl Catal A 221:367–377
2. Nagai K, Ui T (2004) Sumitomo Chem 2:4–13
3. Spivey JJ, Gogate MR, Zoeller JR, Colberg RD (1997) Ind Eng chem Res 36:4600–4608
4. Kanno M, Yasukawa T, Ninomiya W, Ooyachi K, Kamiya Y (2010) J Catal 273:1–8
5. Langpape M, Millet JMM (2000) Appl Catal A 200:89–101
6. Brückner A, Scholz G, Heidemann D, Schneider M, Herein D, Bentrup U, Kant M (2007) J Catal 245:369–380
7. Mestl G, Ilkenhans T, Spielbauer D, Dieterle M, Timpe O, Kröhnert J, Jentoft F, Knözinger H, Schlögl R (2001) Appl Catal A 210:13–34
8. Zhou LL, Wang L, Zhang SJ, Yan RY, Diao YY (2015) J Catal 319:431–440
9. Ai M (1990) Bull Chem Soc Jpn 63:3722–3724
10. Ai M (2005) Appl Catal A 288:211–215
11. Li B, Yan RY, Wang L, Diao YY, Li ZX, Zhang SJ (2013) Catal Lett 143:829–838
12. Li B, Yan RY, Wang L, Diao YY, Li ZX, Zhang SJ (2014) Ind Eng Chem Res 53:1386–1394
13. Gogate MR, Spivey JJ, Zoeller JR (1997) Catal Today 36:243–254
14. Loghmani MH, Shojaei AF (2015) Int J Hydrogen Energy 40:6573–6581
15. Shu YY, Travert A, Schiller R, Ziebarth M, Wormsbecher R, Cheng WC (2015) Top Catal 58:334–342
16. Zhang G, Hattori H, Tanabe K (1988) Appl Catal 36:189–197
17. Chan KS, Ma J, Jaenicke S, Chuah GK, Lee JY (1994) Appl Catal A 107:201–227
18. Song KS, Kang SK, Kim SD (1997) Cattl Lett 45:65–68
19. Sfeir J, Buffat PA, Möckli P, Xanthopoulos N, Vasquez R, Mathieu HJ, Van Herle J, Thampi KR (2001) J Catal 202:229–244
20. Avert PV, Weckhuysen BM (2004) Phys Chem Chem Phys 6:52–56
21. Bhargav KK, Ram S, Labhsetwar N, Majumder SB (2015) Sensor Actuat B 206:389–398

22. Nakamura T, Petzow G, Gauckler LJ (1979) Mater Res Bull 14:649–659
23. Zwinkels MFM, Järås SG, Menon PG, Griffin TA (1993) Catal Rev 35:319–358
24. Kumar P, Srivastava VC, Mishra IM (2015) Catal Commun 60:27–31
25. Nguyen TTN, Ruaux V, Massin L, Lorentz C, Afanasiev P, Maugé F, Bellière-Baca V, Rey P, Millet JMM (2015) Appl Catal B 166–167:432–444
26. Zhao DY, Huo QS, Feng J, Chmelka BF, Stucky GD (1998) J Am Chem Soc 120:6024–6036
27. Russbueldt BM, Hoelderich WF (2010) J Catal 271:290–304
28. Karppinen M, Kyläkoski P, Niinistö L, Rodellas C (1989) J Therm Anal 35:347–353
29. Wang Y, Zhang GF, Li CS, Yan G, Lu YF (2011) Bull Mater Sci 34:1379–1383
30. Nicholson KT, Zhang KZ, Banaszak Holl MM (1999) J Am Chem Soc 121:3232–3233
31. Maileanu M, Crisan M, Petrache C, Crisan D, Jitianu A, Predoi D, Kuncser V, Filoti G (2005) J Phys 50:595–606
32. Gadzhiev AZ, Gafurov MM, Kirillov SA (1980) J Appl Spectrosc 33:1343–1346
33. Gobichon AE, Auffrédic JP, Louër D (1996) Solid State Ion 93:51–64
34. Chen H, Xue MW, Hu SH, Shen JY (2012) Chem Eng J 181–182:677–684
35. Hu SH, Xue MW, Chen H, Shen JY (2010) Chem Eng J 162:371–379
36. Meloni D, Sini MF, Cutrufello MG, Monaci R, Rombi E, Ferino I (2013) J Therm Anal Calorim 112:489–498
37. Gao J, Hou ZY, Guo JZ, Zhu YH, Zheng XM (2008) Catal Today 131:278–284